GATA3 and MDM2 are synthetic lethal in estrogen receptor-positive breast cancers

Gaia Bianco[1], Mairene Coto-Llerena[1,2], John Gallon[1], Stephanie Taha-Mehlitz[1], Venkatesh Kancherla[2], Martina Konantz[3], Sumana Srivatsa[4], Hesam Montazeri[2,5], Marta De Menna[6], Viola Paradiso[1,2], Caner Ercan[2], Niko Beerenwinkel[4], Marianna Kruithof-de Julio[6], Luigi M. Terracciano[2], Claudia Lengerke[3], Rinath M. Jeselsohn[7], Charlotte K. Y. Ng[2,8*] and Salvatore Piscuoglio[1,2*]

Affiliations

[1]Visceral Surgery Research Laboratory, Department of Biomedicine, University of Basel, Basel, Switzerland;

[2]Institute of Medical Genetics and Pathology, University Hospital Basel, Basel, Switzerland;

[3]Department of Biomedicine, University of Basel and University Hospital Basel, Basel, Switzerland;

[4]Department of Biosystems Science and Engineering, ETH Zurich, Basel, Switzerland;

[5]Department of Bioinformatics, Institute of Biochemistry and Biophysics, University of Tehran, Tehran, Iran;

[6]Department of Biomedical Research, Urology Group, University of Bern, Bern, Switzerland;

[7]Division of Women's Cancers, Dana-Farber Cancer Institute, Harvard Medical School. Boston. USA;

[8]Department for BioMedical Research (DBMR), University of Bern, Bern, Switzerland.

Running title: Synthetic lethality of GATA3 and MDM2 in breast cancer

Keywords: *MDM2*, *GATA3*, breast cancer, nutlins, synthetic lethality

Financial support: This work was supported by the Swiss Centre for Applied Human Toxicology; the Swiss Cancer League [KLS-3639-02-2015 to L.M.T., KFS-4543-08-2018 to

C.K.Y.N., KFS-3995-08-2016 to S.P.]; the Swiss National Science Foundation [31003A_169352 to M.K.-d.J.; PZ00P3_168165 to S.P.]; the Dutch Cancer Society [KWF 2015_7599 to M.K.-d.J.]; Novartis [17B076 to M.K.-d.J.]; and the European Research Council [Synergy Grant 609883 to N.B.]. The funders had no role in study design, data collection and analysis, decision to publish, or preparation of the manuscript.

***Corresponding authors: Dr. Salvatore Piscuoglio**, Department of Biomedicine, Basel, Hebelstrasse, 20, 4031, Switzerland; Tel: +41 (0)61 328 6874; Fax: +41 (0)61 2653194. E-mail: s.piscuoglio@unibas.ch and to **Dr. Charlotte K Y Ng**. Department of BioMedical Research, University of Bern, Murtenstrasse 40, CH-3008 Bern, Switzerland; Tel: +41 (0)31 632 8779; Email: charlotte.ng@dbmr.unibe.ch.

Conflict of interest disclosure statement: Part of this study has been submitted for a patent application (applicants: University of Basel and ETH Zürich; the name of the inventors: G.B, S.S., H.M., N.B., C.K.Y.N. and S.P. The patent application has been submitted to the European patent office; application number: EP19216550.4). The other authors declare no competing interests.

Word count: 5386; Number of Figures: 5

Abstract

Synthetic lethal interactions, where the simultaneous but not individual inactivation of two genes is lethal to the cell, have been successfully exploited to treat cancer. *GATA3* is frequently mutated in estrogen receptor (ER)-positive breast cancers and its deficiency defines a subset of patients with poor response to hormonal therapy. However, GATA3 is not targetable. Here we show that GATA3 and MDM2 are synthetically lethal in ER-positive breast cancer. Depletion and pharmacological inhibition of MDM2 induce apoptosis in *GATA3*-deficient models *in vitro* and *in vivo*. The synthetic lethality requires p53 and acts via the PI3K/Akt/mTOR pathway. Our results present MDM2 as a novel therapeutic target in the substantial cohort of ER-positive, *GATA3*-deficient breast cancer patients. With MDM2 inhibitors widely available, our findings can be rapidly translated into clinical trials to evaluate in-patient efficacy.

Statement of significance

GATA3 mutations are common in ER-positive breast cancers yet are not targetable. Our findings describe pharmacological inhibition of MDM2 as a novel approach to target GATA3 deficiency, providing a molecularly guided treatment for this patient subclass associated with a worse prognosis and relapse.

Introduction

GATA3 is mutated in 12-18% of primary and metastatic estrogen receptor (ER)-positive breast cancers, with predominantly frameshift mutations and mutations affecting splice sites (1,2). It is the most highly expressed transcription factor in the mammary epithelium (3) and has key functions in mammary epithelial cell differentiation (3). In breast cancer, GATA3 suppresses epithelial-to-mesenchymal transition (4) and acts as a pioneer transcription factor by recruiting other cofactors such as ERα and FOXA1 (5,6). Its expression level is strongly associated with ERα expression and is diagnostic of the luminal A and luminal B subtypes. Indeed, GATA3 loss has also been strongly linked to poor response to hormonal therapy and poor prognosis (7–9). Therefore, targeting GATA3 deficiency may provide a specific and tailored treatment for a subclass of patients associated with a worse prognosis and relapse.

Synthetic lethality refers to the interaction between genetic events in two genes whereby the inactivation of either gene results in a viable phenotype, while their combined inactivation is lethal (10). It has helped extend precision oncology to targeting genes with loss-of-function mutations by disrupting the genetic interactors of the mutated gene. One such example is the use of poly(ADP-ribose) polymerase (PARP) inhibition in cancers with deficiencies in homologous recombination (11). Recent developments in large-scale perturbation screens have enabled the comprehensive screening of genetic interactions (12) and the systematic analysis of these screens has led to the discovery of further synthetic lethal targets in cancer (13,14). In this study, using our recently developed SLIdR (Synthetic Lethal Identification in R) algorithm (15), we systematically interrogate the project DRIVE RNAi screen (12) and identify MDM2 as a synthetic lethal interactor of GATA3 in ER-positive breast cancer. We show that inhibition of MDM2 is synthetically lethal in *GATA3*-mutant (loss-of-function) and GATA3-depleted breast cancer cells. Our findings establish a new approach for targeting GATA3 deficiency in ER-positive breast cancer by pharmacological inhibition of MDM2 using

selective small molecules which are currently being evaluated in Phase III clinical trials in haematological malignancies (e.g. NCT02545283).

Results

GATA3 and *MDM2* are synthetic lethal in ER-positive breast cancer

To identify synthetically lethal vulnerabilities of *GATA3* in breast cancer, we analyzed the breast cancer cell line (n=22) data from the large-scale, deep RNAi screen project DRIVE (12) (**Fig. 1A**) using our recently developed SLIdR algorithm (15). SLIdR uses rank-based statistical tests to compare the viability scores for each gene knock-down between the *GATA3*-mutant and *GATA3*-wild type cell lines and identified *MDM2* as the top gene whose knock-down significantly reduced cell viability in the two *GATA3*-mutant breast cancer cell lines (**Fig. 1B-C**). *MDM2* encodes an E3 ubiquitin ligase that inhibits the tumor suppressor p53-mediated transcriptional activation (16) and is frequently amplified and overexpressed in human cancers, including breast (17).

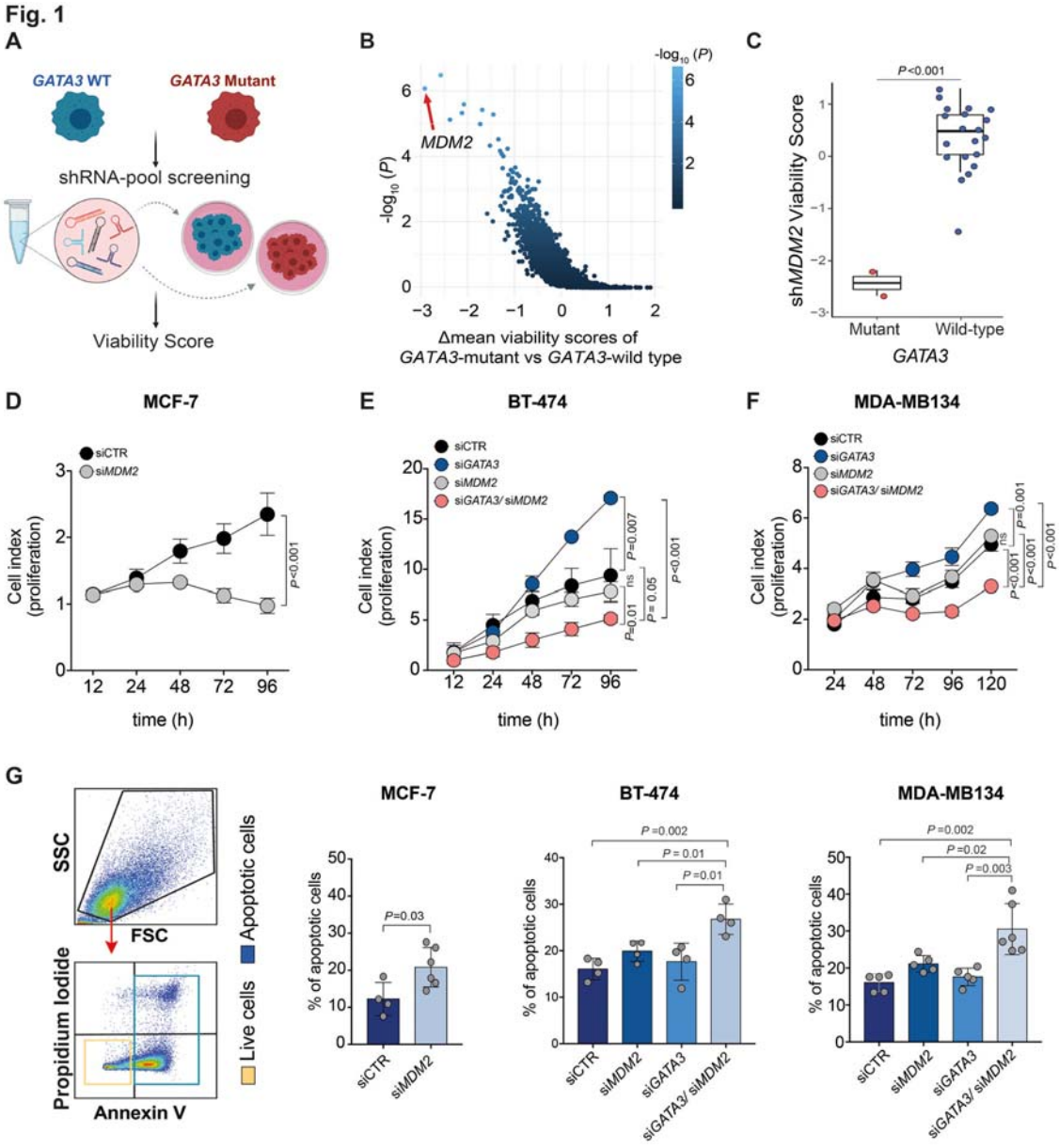

Fig. 1: *GATA3* and *MDM2* are synthetic lethal in ER-positive breast cancer. (A) Schematic representation of the project DRIVE shRNA screen data used to identify synthetic lethal interactors of *GATA3*. **(B)** SLIdR-derived statistical significance ($-\log_{10}(P)$) plotted against the difference in the mean viability scores between *GATA3*-mutant and *GATA3*-wild type breast cancer cell lines for each gene knocked-down in the shRNA screen. Middle lines of the boxplots indicate medians. Box limits are first and third quartiles. The whiskers extend to the range. **(C)** Viability scores of *MDM2* knock-down in *GATA3*-mutant and *GATA3*-wild type cell lines. **(D-F)** Proliferation kinetics of **(D)** *GATA3*-mutant MCF-7 transfected with siRNA targeting *MDM2* or control, **(E)** *GATA3*-wild type BT-474, **(F)** *GATA3*-wild type MDA-MB134 transfected with siRNA targeting *GATA3, MDM2, GATA3/ MDM2,* or control. **(G)** Apoptosis assay using Annexin V and propidium iodide co-staining. From left: gating strategy to define apoptotic (yellow) and live (blue) cells; percentage of apoptotic and live cells upon *MDM2* silencing in MCF-7; upon silencing of *GATA3* or *MDM2* alone or in combination in BT-474 and MDA-MB134. Data are mean ± s.d. **(D,E,F,G)** n≥4 replicates.

Statistical significance was determined for **(D,E,F,G)** by the two-tailed unpaired Student's t-test.

We first sought to validate the predicted synthetic lethality between *GATA3* and *MDM2* in the ER-positive breast cancer cell line MCF-7, one of the two *GATA3*-mutant cell lines used in the RNAi screen (12). MCF-7 harbors the *GATA3* frameshift mutation p.D335Gfs (18), a loss-of-function mutation that has been recurrently observed in breast cancer patients (1,19) and leads to a truncated GATA3 protein. Using a siRNA approach, we confirmed that silencing *MDM2* significantly reduced cell proliferation in MCF-7 cells (**Fig. 1D, Supplementary Fig. S1A**). *MDM2* siRNA titration analysis showed that the vulnerability induced by *MDM2* inhibition in MCF-7 was dose-dependent and that 50% reduction in *MDM2* expression is sufficient to inhibit proliferation in the presence of *GATA3* mutation (**Supplementary Fig. S1B-C**).

To confirm that the effect of *MDM2* silencing is unequivocally related to GATA3 loss of function and to exclude any gain-of-function effects of the *GATA3* mutation, we assessed the changes in cell proliferation upon single- and dual-silencing of *GATA3* and *MDM2* using siRNA in two ER-positive *GATA3*-wild type breast cancer cell lines; the luminal A (ER+/HER2-) MDA-MB134 and the luminal B (ER+/HER2+) BT-474 (**Supplementary Fig. S2**). Consistent with the oncosuppressor role of *GATA3* in breast cancer (20,21), *GATA3*-silencing led to a significant increase in cell proliferation in both BT-474 and MDA-MB134 (**Fig. 1E-F**). By contrast, dual-silencing of *GATA3* and *MDM2* significantly reduced cell proliferation compared to cells transfected with control siRNA, *GATA3* siRNA or *MDM2* siRNA alone (**Fig. 1E-F**).

To determine if *MDM2* silencing was merely inhibiting cell growth or was inducing cell death, we assessed apoptosis using Annexin V and propidium iodide co-staining followed by flow cytometry analysis. We observed that *MDM2* silencing significantly induced apoptosis in MCF-7 cells in a dose-dependent manner (**Fig. 1G, Supplementary Fig. S1D**). Similarly,

dual-*GATA3*/*MDM2* silencing in BT-474 and MDA-MB134 cells led to 15-20% higher proportion of apoptotic cells than the silencing of the two genes individually (**Fig. 1G**), indicating that dual inhibition induced increased apoptosis.

Our results provide evidence that MDM2 is a selected vulnerability in breast cancer with *GATA3*-mutation and/or loss of *GATA3*.

GATA3 status determines response to MDM2 inhibitor *in vitro*

The selected vulnerability of MDM2 in *GATA3*-deficient ER-positive breast cancers presents MDM2 as an attractive therapeutic target in this patient cohort. To test whether the apoptotic effects of MDM2 inhibition could be achieved using an MDM2 antagonist, we treated the breast cancer cell lines with idasanutlin (RG7388 (22,23)). In the *GATA3*-mutant MCF7 cells, idasanutlin induced cell growth arrest and apoptosis in a dose-dependent manner (**Fig. 2A-B, Supplementary Fig. S3A**). To assess if idasanutlin was inducing the canonical apoptotic cascade, we assessed the expression of p53, Bax and Bcl-2, together with the canonical markers of apoptosis PARP and cleaved PARP, by immunoblot at 6, 12 and 24 hours post-treatment. Idasanutlin induced an early up-regulation of p53 and MDM2 proteins (24), together with the up- and down-regulation of pro- and anti-apoptotic proteins, respectively (**Fig. 2C**), leading to the activation of the apoptotic cascade.

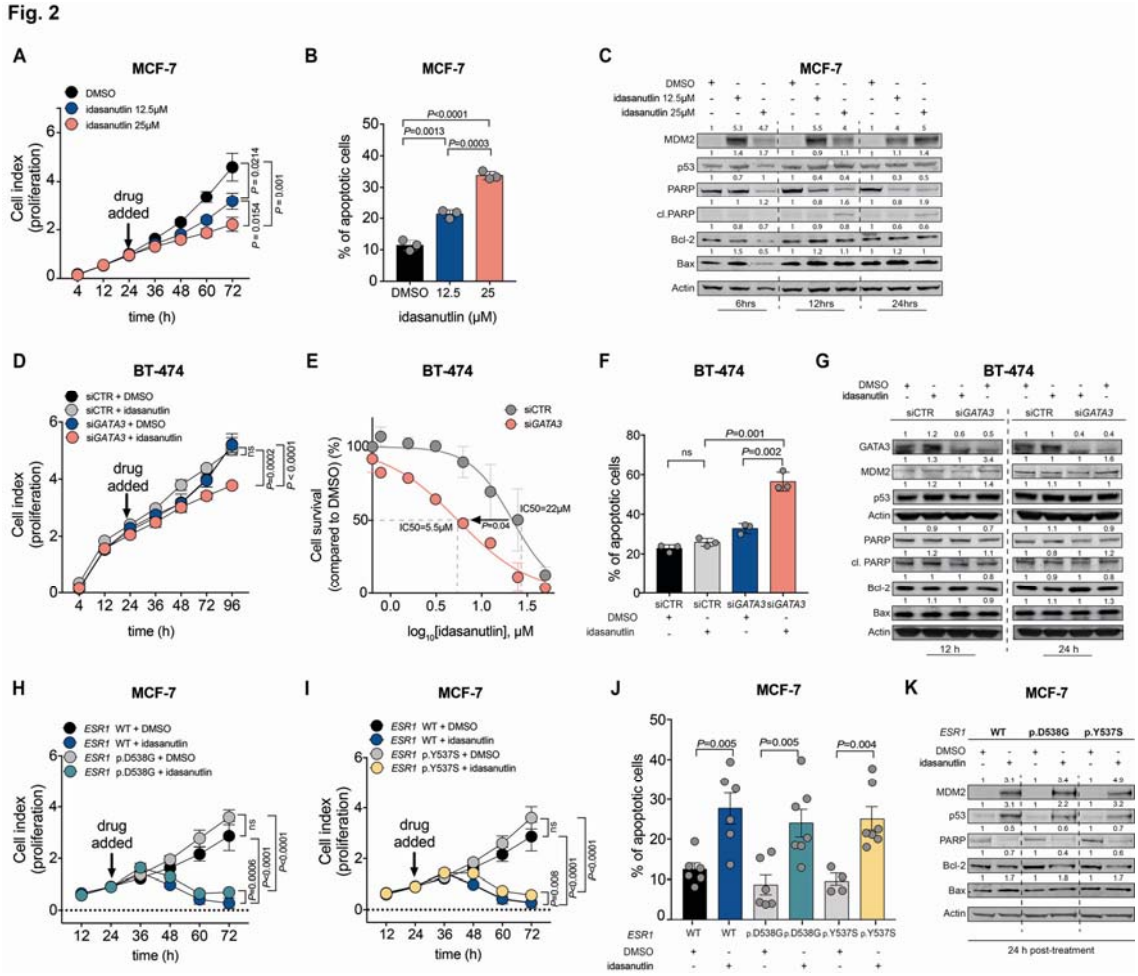

Fig. 2: *GATA3* status determines response to MDM2 inhibitors *in vitro*. (A,D,H,I) Proliferation kinetics of **(A)** *GATA3*-mutant MCF-7 under increasing dosage of idasanutlin, **(D)** BT-474 upon *GATA3* silencing and/or treatment with 12.5 μM idasanutlin, **(H,I)** *GATA3*-mutant MCF-7 carrying a wild-type *ESR1* or mutant *ESR1* (p.D538G/p.Y537S) upon treatment with 12.5 μM idasanutlin. **(B,F,J)** Apoptosis assay using Annexin V and propidium iodide co-staining **(B)** upon increasing dosage of idasanutlin in MCF-7, **(F)** upon *GATA3* silencing and/or treatment with 12.5 μM idasanutlin in BT-474, **(J)** upon treatment of 12.5 μM idasanutlin in MCF-7 carrying a wild-type *ESR1* or mutant *ESR1* (p.D538G/p.Y537S). **(C,G,K)** Immunoblot showing pro- and anti-apoptotic proteins **(C)** at 6, 12 and 24 h post-treatment with DMSO, 12.5 μM and 25 μM idasanutlin in MCF-7, **(G)** at 12 and 24 h post-treatment with DMSO or 12.5 μM idasanutlin in BT-474 transfected with *GATA3* siRNA or control siRNA, **(K)** at 24 h post-treatment with DMSO or 12.5 μM idasanutlin in MCF-7 carrying wild-type or mutant *ESR1* (p.D538G/p.Y537S). For all the western blots, quantification is relative to the loading control (actin) and normalized to the corresponding DMSO control. Data are mean ± s.d. **(A,B,D,E,F,H,I,J)** n≥3 replicates. Statistical significance was determined for **(A,B,D,E,F,H,I,J)** by the two-tailed unpaired Student's t-test.

To determine whether *GATA3* expression levels would modulate response to idasanutlin, we assessed the effect of treatment on *GATA3*-silenced BT-474 and MDA-MB134 cells. We observed that while idasanutlin treatment had no or little effect on the proliferation of the

control cells, it significantly reduced cell proliferation upon *GATA3* silencing **(Fig. 2D, Supplementary Fig. S3B**). In fact, both cell lines showed that *GATA3* silencing substantially reduced the IC50 for idasanutlin **(Fig. 2E, Supplementary Fig. S3C).** Flow cytometry and immunoblot further demonstrated that idasanutlin treatment induced apoptosis in both BT-474 and MDA-MB134 upon *GATA3* silencing but not in control cells (**Fig. 2F-G, Supplementary Fig. S3D-E**).

Acquired resistance to endocrine therapy is often associated with *ESR1* activating mutations (25) or fusion genes (26). We hypothesized that *MDM2* inhibition may represent an alternative therapeutic strategy in endocrine therapy-resistant breast cancers harboring *GATA3* mutations. To test this hypothesis, we treated two derivative endocrine-resistant *GATA3*-mutant MCF-7 cell lines with knock-in *ESR1* p.D538G or p.Y537S activating mutations (27,28) with idasanutlin. We observed that idasanutlin stopped cell proliferation in both mutant cell lines (**Fig. 2H-I**). Idasanutlin also induced apoptosis and up- and down-regulated pro- and anti-apoptotic proteins, respectively (**Fig. 2J-K**).

Taken together, our results demonstrate that *GATA3* loss sensitizes cells to pharmacological inhibition of MDM2 *in vitro*.

GATA3 expression determines response to MDM2 inhibitor *in vivo*

To ascertain whether *GATA3* expression levels would also modulate response to idasanutlin *in vivo*, we performed xenotransplantation into zebrafish embryos. As a cancer model system, human cancer xenografts in zebrafish recapitulate the response to anticancer therapies of mammalian models (29,30). To generate the zebrafish models, we treated *GATA3*-silenced and control BT-474 cells with idasanutlin (25 μM) or vehicle (DMSO) 48 hours post-siRNA transfection (**Fig. 3A**). Twenty-four hours later, we labeled the cells with a red fluorescent cell tracker, injected them into the yolk sac of zebrafish embryos and screened embryos for tumor cell engraftment after four days (31).

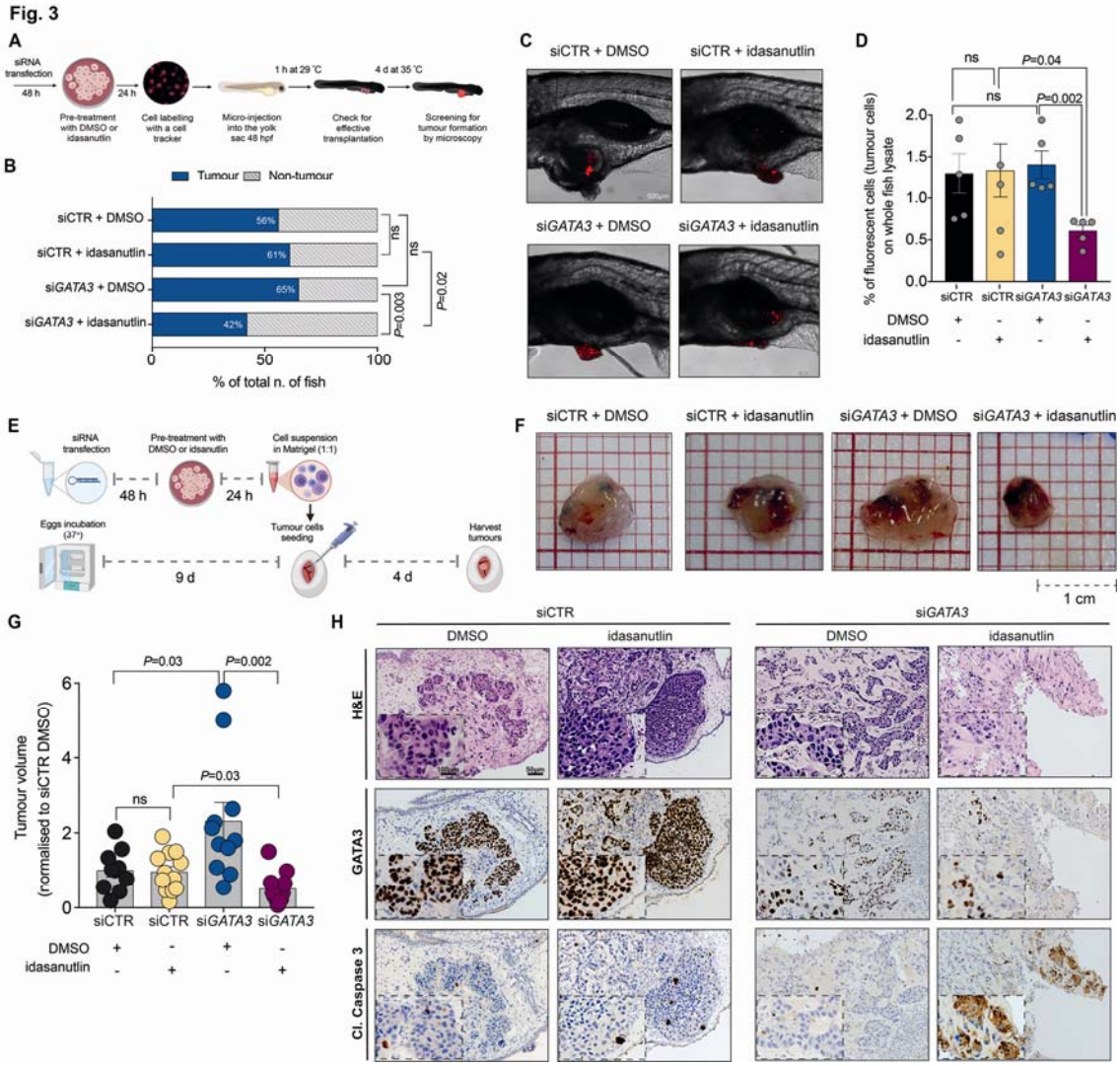

Fig. 3: GATA3 expression determines response to MDM2 inhibitor *in vivo.* **(A)** Schematic representation of the zebrafish xenotransplantation assay. **(B)** Barplot shows the percentages of fish that harbored or did not harbor tumors upon transplantation with *GATA3*-silenced or control BT-474 cells pre-treated with idasanutlin or DMSO. In total, 70-100 embryos per group were analyzed over two independent experiments. **(C)** Representative confocal images of tumor formation in zebrafish injected with fluorescent tracker-labeled BT-474 cells with *GATA3* siRNA or control siRNA, pretreated with idasanutlin or DMSO. **(D)** FACS analysis showing the percentage of red-tracker labelled tumor cells extracted from the embryos. Error bars represent, in total, three replicates performed over two independent experiments. Each replicate represents the pooled lysate of 20-30 fish for each condition. **(E)** Schematic illustration of the CAM assay. **(F)** Photographs of *GATA3*-silenced or control BT-474 cells pre-treated with DMSO or idasanutlin implanted in CAMs and grown for four days post-implantation. **(G)** Volume of tumors derived from the CAM experiment (n≥10 tumors over three independent experiments). Values are normalized to the mean of siCTR DMSO. **(H)** Representative micrographs of BT-474 tumors extracted four days post-implantation. Tumoral cells (upper) were immunostained with GATA3 (middle) and the apoptotic marker cleaved caspase 3 (lower) in the different treatment conditions. Data are mean ± SEM **(D,G)**

n≥4 replicates. Scale bars: **(C)** 500 µm**, (F)** 1cm and **(H)** 50 µm and 100 µm**.** Statistical significance was determined for **(B)** by two-sided Fisher's Exact test and for **(D,G)** by the two-tailed unpaired Student's t-test.

We observed that *GATA3*-silenced cells injected into fish were more sensitive to idasanutlin than the control (42% vs 61%, **Fig. 3B**). More importantly, idasanutlin reduced tumor formation in the context of *GATA3*-silencing (42% vs 65% treated with DMSO) but not in control (61% vs 56% treated with DMSO, **Fig. 3B**). Tumors derived from *GATA3*-silenced, idasanutlin-treated cells, were very small, largely consisting of small clusters of tumor cells, compared to the larger solid tumor masses derived from *GATA3*-silenced cells without idasanutlin (**Fig. 3C**). To assess cell proliferation, we quantified the percentage of tumor cells present in the fish by performing FACS analysis of the fluorescence-labeled tumor cells in whole fish extracts. Consistent with the results from the tumor formation assay, idasanutlin treatment was only effective in reducing the overall percentage of tumor cells in fish injected with *GATA3*-silenced cells (purple vs DMSO-treated in blue) but not in fish injected with control (yellow vs DMSO-treated in black, **Fig. 3D**), indicating that *GATA3* expression level modulates sensitivity to MDM2 inhibition *in vivo*.

The zebrafish xenograft model provides insights into the tumorigenic and proliferative capability of cancer cells. However, to assess apoptosis and to quantify tumor growth, we employed the chicken chorioallantoic membrane (CAM), a densely vascularized extraembryonic tissue, as a second *in vivo* model (32,33). Similar to the zebrafish assay, we treated *GATA3*-silenced and control BT-474 cells with idasanutlin (25 µM) or vehicle (DMSO) for 24 hours (**Fig. 3E**). We then inoculated the cells into the CAMs and screened the eggs for tumor formation four days later. In accordance with our results in the zebrafish model, idasanutlin treatment reduced the volume of tumors formed by *GATA3*-silenced cells (purple vs DMSO-treated in blue) but not in control cells (yellow vs DMSO-treated in black, **Fig, 3F-G**), suggesting that *GATA3* expression modulates response to MDM2 inhibitors in the CAM model as well. We then evaluated apoptosis induction by staining tumor sections

with the apoptotic marker cleaved caspase 3. Notably, only *GATA3*-silenced idasanutlin-treated tumors showed a strong positive signal for cleaved caspase 3, as well as morphological features of apoptosis (e.g. nuclear fragmentation, hypereosinophilic cytoplasm, "apoptotic bodies", **Fig. 3H, Supplementary Fig. S4**), demonstrating that idasanutlin induces apoptosis in the context of *GATA3* silencing *in vivo*. Taken together, our results show that *GATA3* expression modulates response to idasanutlin in two independent *in vivo* models.

The synthetic lethality between *GATA3* and *MDM2* is *TP53* dependent

MDM2 plays a central role in the regulation of p53 and they regulate each other in a complex regulatory feedback loop (34) (**Fig. 4A**). We analyzed the frequencies of *GATA3* and *TP53* mutations in ER-positive breast cancer (1,19) and observed that they are mutually exclusive (**Fig. 4B**). We, therefore, hypothesized that the synthetic lethal effects between *GATA3* and *MDM2* may be p53-dependent. To test this hypothesis, we assessed cell growth and apoptosis upon single- and dual-silencing of *GATA3* and *MDM2* in the ER-positive, *GATA3*-wild-type, *TP53*-mutant (p.L194F) T-47D breast cancer cell line (**Supplementary Fig.S5A**). Consistent with the mutual exclusivity of *GATA3* and *TP53* mutations, *GATA3* silencing in a *TP53*-mutant context resulted in a strong reduction of cell viability and induction of apoptosis (**Fig. 4C-D**). Contrary to the results obtained in cells with functional p53, *GATA3*/*MDM2* dual silencing did not show synthetic lethal effect (**Fig. 4C-D**). If the synthetic lethal interaction between *GATA3* and *MDM2* is *TP53*-dependent, one should expect that silencing *TP53* should partially revert the phenotype. Therefore, we silenced *MDM2* alone or in combination with *TP53* in the *GATA3*-mutant MCF-7 cell line (**Supplementary Fig. S5B**). As expected, *TP53* silencing partially rescued the effect induced by *MDM2* knock-down (**Fig. 4E-F**) as well as of idasanutlin treatment (**Fig.4G-H, Supplementary Fig. S5C-D**) on cell growth and apoptosis, demonstrating the p53 dependency of the synthetic lethal interaction.

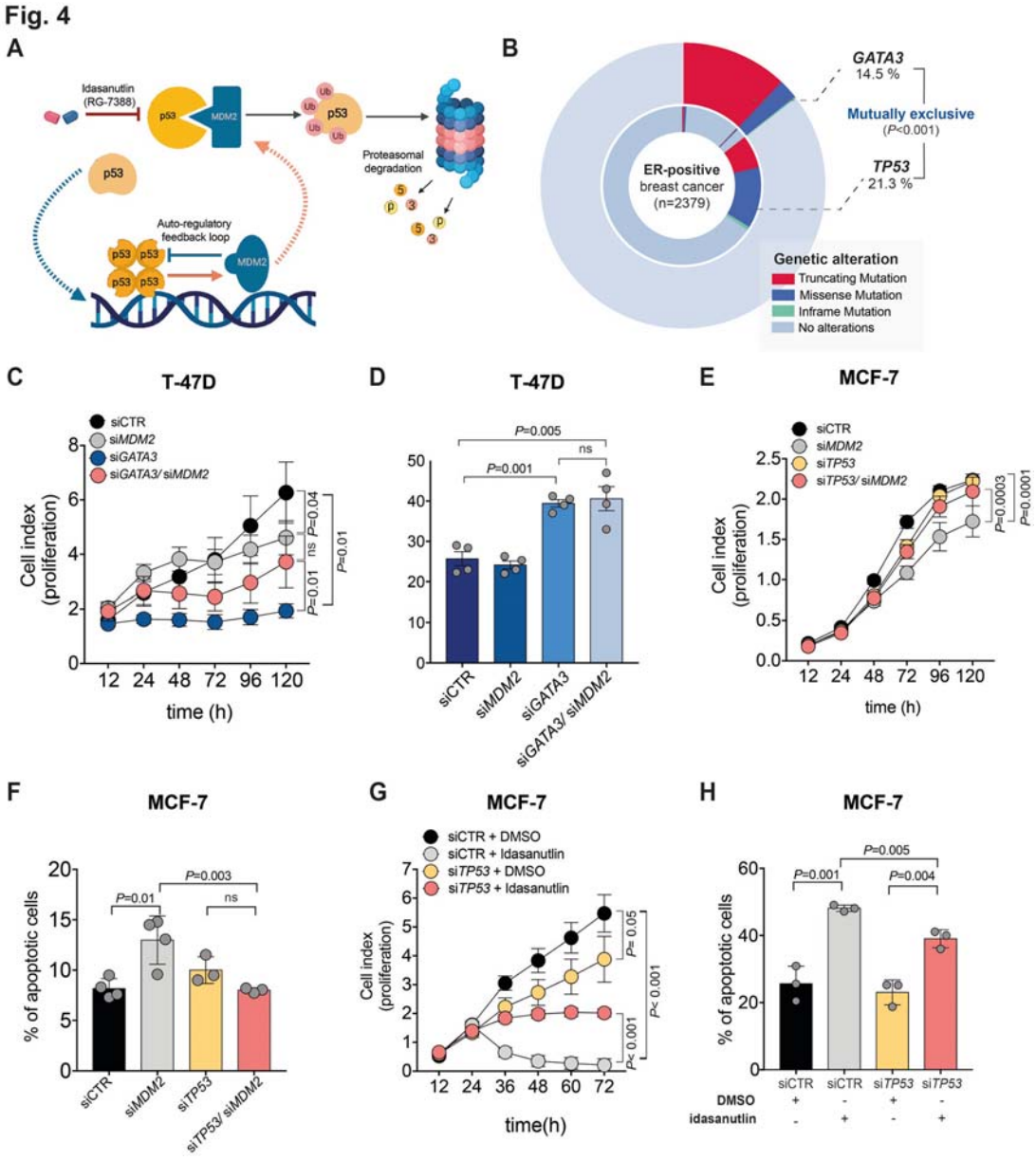

Fig. 4: The synthetic lethality between *GATA3* and *MDM2* is *TP53* dependent. (A) Schematic representation on the regulatory feedback loop between MDM2 and p53. (**B**) Doughnut chart showing *GATA3* and *TP53* mutations in ER-positive breast cancer(1,19). (**C**)Proliferation kinetic of *TP53*-mutant T-47D transfected with siRNA targeting *GATA3, MDM2, GATA3/ MDM2,* or control. **(D)** Percentage of apoptotic and live cells upon silencing of *GATA3* and *MDM2* alone or in combination in T-47D. **(E)** and for **(H)** by one-sided Fisher's Exact test.

The synthetic lethality between *GATA3* and *MDM2* acts via the PI3K-Akt-mTOR signaling pathway

To investigate the putative mechanisms driving the synthetic lethality, we analyzed the gene expression changes induced by concurrent *GATA3* loss and *MDM2* silencing. RNA-sequencing analysis of the *MDM2*-silenced MCF-7 cells and dual *GATA3/MDM2*-silenced MDA-MB134 cells revealed 20 commonly dysregulated pathways (**Fig. 5A**). As expected, pathways related to p53 and apoptosis were significantly up-regulated in both cell lines, while many proliferation-related pathways such as *E2F* and *MYC* targets were down-regulated (**Fig. 5B**). Interestingly, the mTORC1 signaling pathway was among the most significantly down-regulated pathways in both cell lines. Indeed, we confirmed that *MDM2* silencing in the *GATA3*-mutant MCF7 cells (**Supplementary Fig.S6A**) reduced phospho-Akt, phospho-S6, as well as phospho-GSK3β, compared to control cells (**Fig. 5C**), indicating the down-regulation of the mTOR pathway. Similarly, in BT-474 cells, dual *GATA3/MDM2* silencing reduced levels of phospho-Akt, phospho-S6 and phospho-GSK3β and induced apoptosis (**Fig. 5D and Supplementary Fig. S6A**)**.** By contrast, phospho-Akt levels were higher when only *GATA3* was silenced (**Fig. 5D and Supplementary Fig. S6B**). Pharmacological inhibition of MDM2 in *GATA3*-silenced BT-474 cells also resulted in a reduction in phospho-Akt, phospho-S6 and phospho-GSK3β (**Supplementary Fig. S6B**). To determine whether activation of the mTOR signaling could also be observed *in vivo*, we stained the tumors in our CAM model with phospho-S6 and phospho-Akt. Indeed, in tumors derived from *GATA3*-silenced BT-474 cells, both phospho-S6 and phospho-Akt were drastically reduced upon treatment with idasanutlin, while in tumors derived from control cells, idasanutlin treatment did not have an effect on mTOR signaling (**Fig. 5E**, **Supplementary Fig. S6C**).

Fig. 5

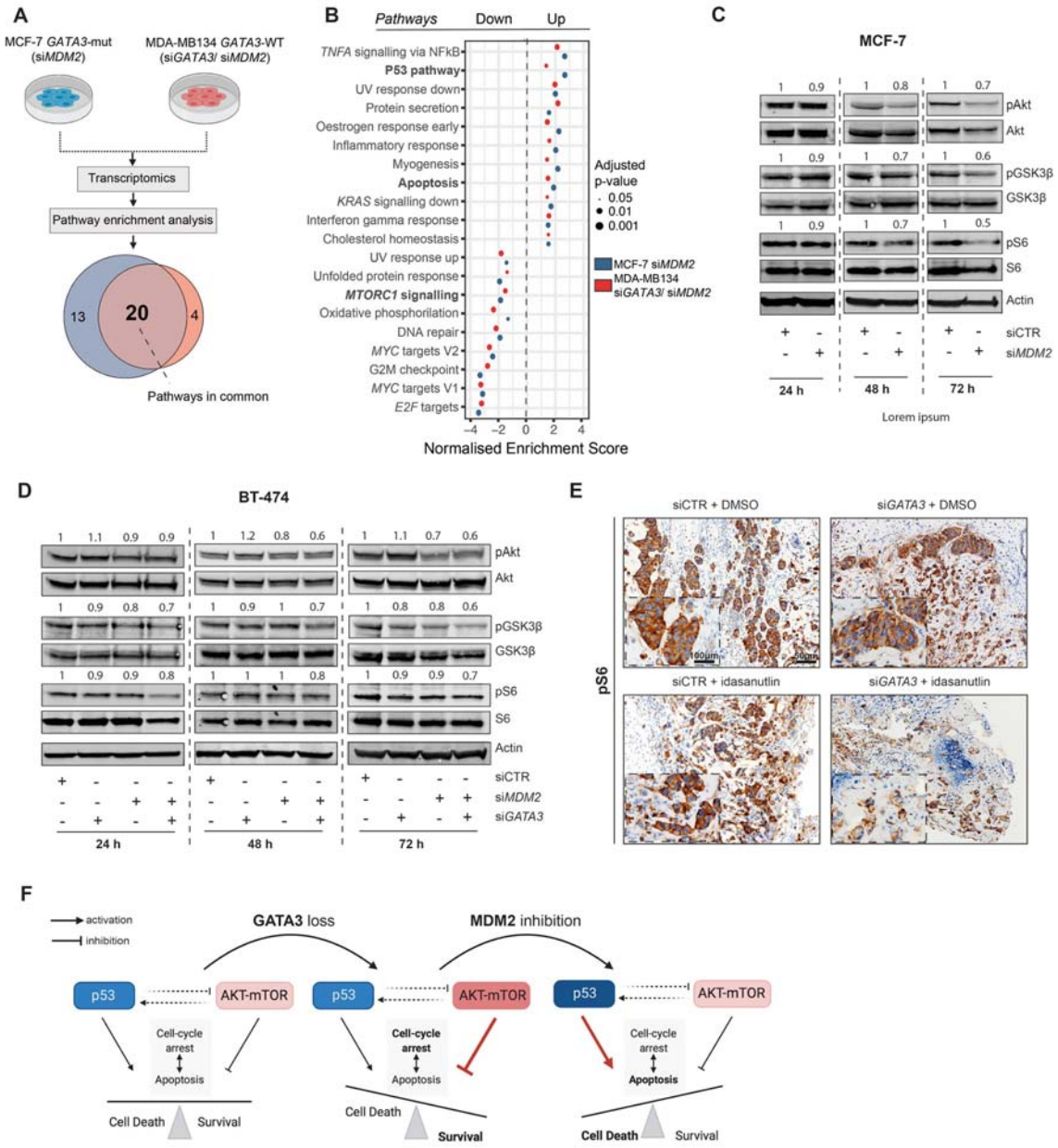

Fig. 5: The synthetic lethality between *GATA3* and *MDM2* acts via the PI3K-Akt-mTOR signaling pathway. (A) Schematic representation of the RNA-seq experimental setup to identify gene expression changes induced by concurrent *GATA3* loss and *MDM2* inhibition. Venn diagram shows the number of pathways enriched in both MCF-7 with *MDM2* siRNA and MDA-MB134 with *GATA3* siRNA and *MDM2* siRNA. **(B)** Normalized enrichment scores of significantly up- and down-regulated pathways identified by gene set enrichment analysis in both MCF-7 and MDA-MB134. Size of the dots is proportional to the adjusted p-value as indicated in the legend. **(C,D)** Immunoblot showing markers of mTOR signaling pathway activation at 24, 48 and 72 hours post-siRNA transfection in **(C)** MCF-7 cells upon *MDM2* silencing and **(D)** BT-474 cells upon *GATA3* and/or *MDM2* silencing. For all the western blots, quantification is relative to the loading control (actin) and normalized to the corresponding siCTR. **(E)** Representative immunohistochemistry micrographs of phospho-

S6 stainings in BT-474 tumors extracted four days post-implantation in the CAM model. **(F)** Schematic representation of the mechanistic hypothesis. Scale bars: **(E)** 50 µm and 100 µm. Statistical significance was determined for **(B)** by *fgsea*.

We, therefore, hypothesized that GATA3 loss may induce addiction to mTOR signaling in breast cancer cells. In support of our hypothesis, we observed that, in ER-positive breast cancers, genetic alterations in *GATA3* are significantly mutually exclusive with those in both *PI3KCA* and *PTEN* (**Supplementary Fig. S7A-B**). Furthermore, differential gene expression and pathway enrichment analyses between *GATA3*-mutant and *GATA3*-wild type ER-positive breast cancers and between ER-positive breast cancers with low and high *GATA3* expression levels also showed significant enrichment for the mTORC1 signaling pathway (**Supplementary Fig. S7C-D**). Taken together, our results show that the synthetic lethality between GATA3 and MDM2 acts via the PI3K-Akt-mTOR signaling pathway.

Discussion

GATA3 is mutated in 12-18% of breast cancer (1,2) with predominantly frameshift mutations and loss of GATA3 expression is strongly associated with failure to respond to hormonal therapy and poor prognosis (9). Here we describe a novel synthetic lethal interaction between *GATA3* and *MDM2* in ER-positive breast cancer. In particular, we showed that, in the context of truncating *GATA3* mutation, inhibition of MDM2 hampers cell proliferation and induces apoptosis. In the context of wild-type *GATA3*, the same effect was achieved by dual *GATA3* and *MDM2* inhibition, regardless of HER2 status. We further showed that *GATA3* expression level modulates response to MDM2 inhibitor *in vitro* and in two independent *in vivo* models. Our results thus support MDM2 as a therapeutic target in the substantial fraction of ER-positive, *GATA3*-deficient breast cancer. Of note, although *TP53* mutations are a major driver of resistance to MDM2 inhibitors (35,36), very few *GATA3*-mutant ER-positive breast cancers harbor *TP53* mutations. Thus the presence of *TP53* mutations is not expected to preclude the use of MDM2 inhibitors in the vast majority of these patients. With MDM2 inhibitors, such as idasanutlin, widely available, our findings allow the rational design

of clinical trials to evaluate the in-patient efficacy of MDM2 inhibitors and to specifically evaluate GATA3 status as a predictive biomarker of response. Given that GATA3 loss of expression has also been associated with poor prognosis in other cancer types(37,38), we expect our finding to have far-reaching implications beyond ER-positive breast cancer.

We showed that the synthetic lethality between *GATA3* and *MDM2* is p53-dependent and acts via the PI3K/Akt/mTOR pathway. It is well known that in normal conditions p53 and the PI3K/Akt/mTOR pathway co-regulate cell cycle arrest and apoptosis leading to homeostasis between cell death and survival (39,40). Our results suggest that in breast cancer cells, *GATA3* loss-of-function (via genetic alterations or other mechanisms) activates the PI3K/Akt/mTOR pathway and leads to resistance to apoptosis. In this context, MDM2 inhibition, with consequent p53 up-regulation and mTOR signaling down-regulation, pushes the cells toward cell death (**Fig. 5F**). In support of this model, down-regulation of *GATA3* has been directly linked to Akt kinase activation in breast and prostate cancers (38,41,42). It has also been reported that upon adaptation to hormone deprivation, breast cancer cells rely heavily on PI3K signaling and that inhibition of PI3K and mTOR induces apoptosis in these cells (43). Furthermore, our model is also supported by the observed synergistic effect of dual MDM2 and PI3K/Akt/mTOR inhibition (44,45). Our hypothesis, however, may only partially explain the synthetic lethality between GATA3 and MDM2. Further studies are required to fully dissect the mechanism of action.

Our findings have important clinical implications for several subsets of ER-positive breast cancer. First, our findings provide evidence that *GATA3* mutations may drive resistance to hormonal therapy by upregulating the PI3K/Akt/mTOR pathway, suggesting that inhibition of MDM2 may help overcome the resistance in *GATA3*-deficient breast cancer. Second, the mutual exclusivity between genetic alterations in *GATA3* and genes in the PI3K pathway suggests the PI3K inhibitors may be effective in the context of *GATA3* mutations. It would be clinically relevant to test if the synergistic effect of dual MDM2 and PI3K/Akt/mTOR inhibition

is even stronger in the context of *GATA3* mutation. Third, given that aberrant activation of the PI3K pathway has been implicated in resistance to HER2-targeted therapy (46), one might hypothesize that *GATA3* mutations may be a mechanism of resistance to HER2-targeted therapy and that MDM2 inhibitors may act synergistically with trastuzumab in ER+/HER2+, *GATA3*-mutant breast cancers.

Despite the profound therapeutic implications, the synthetic lethality between GATA3 and MDM2 had never been reported. This unexpected finding was the result of the availability of large-scale, unbiased screening of genetic interactions in a large panel of cell lines (12) as well as a statistical algorithm (15) powerful enough to detect such interaction even when the number of cell lines harboring *GATA3* mutation is small (n=2). Our study exemplifies how perturbation screens can lead to pre-clinical hypotheses that can be rapidly tested and translated into therapeutic candidates.

Methods

Cell lines

ER-positive breast cancer cell lines MCF-7 (*GATA3*-mutant p.D335Gfs; *TP53* wild-type), BT-474 (*GATA3* wild-type, *TP53* mutant p.E285K with retained transactivation activity (47)), MDA-MB134 (*GATA3* wild-type; *TP53* wild-type) and T-47D (*GATA3* wild-type, *TP53* mutant p.L194F) were kindly provided by Dr. Rachael Natrajan from The Institute of Cancer Research (London, UK), authenticated by short tandem repeat profiling. MCF-7 cell lines with knock-in mutations in the *ESR1* gene (p.Y537S and p.D538G) were provided by Dr. Jeselsohn (27). All cell lines were monitored regularly for mycoplasma contamination by PCR using specific primers as described previously (48). All cell lines were maintained under the condition as recommended by the provider. Briefly, all cell lines were cultured in DMEM supplemented with 5% Fetal Bovine Serum, non-essential amino-acids and antibiotics (Penicillin/Streptomycin). The cells were incubated at 37°C in a humidified atmosphere containing 5% CO2. Exponentially growing cells were used for all *in vitro* and *in vivo* studies.

Gene knockdown by siRNAs

Transient gene knockdown was conducted using ON-TARGET plus siRNA transfection. ON-TARGET plus SMARTpool siRNAs against human *GATA3*, *MDM2*, *TP53*, ON-TARGET plus SMARTpool non-targeting control and DharmaFECT transfection reagent were all purchased from GE Dharmacon **(Supplementary Table S1)**. Transfection was performed according to the manufacturer's protocol. Briefly, log-phase ER-positive breast cancer cells were seeded at approximately 60% confluence. Because residual serum affects the knockdown efficiency of ON-TARGET plus siRNAs, growth medium was removed as much as possible and replaced by serum-free medium (Opti-MEM). siRNAs were added to a final concentration of 25 nM, unless otherwise specified (Note: siRNAs targeting different genes can be multiplexed). Cells were incubated at 37°C in 5% CO2 for 24, 48 and 72 h (for mRNA analysis) or for 48 and 72 h (for protein analysis). To avoid cytotoxicity, the transfection medium was replaced with a complete medium after 24 h.

RNA extraction and relative expression by qRT-PCR

Total RNA was extracted from cells at 75% confluence using TRIZOL **(Supplementary Table S1)** according to the manufacturer's guidelines. cDNA was synthesized from 1 µg of total RNA using SuperScript™ VILO™ cDNA Synthesis Kit. All reverse transcriptase reactions, including no-template controls, were run on an Applied Biosystem 7900HT thermocycler. The expression for all the genes was assessed using SYBR and all qPCR experiments were conducted at 50°C for 2min, 95°C for 10min, and then 40 cycles of 95°C for 15 s and 60°C for 1min on a QuantStudio 3 Real-Time PCR System (Applied Biosystems). The specificity of the reactions was verified by melting curve analysis. Measurements were normalized using *GAPDH* level as reference. The fold change in gene expression was calculated using the standard ΔΔCt method (49). All samples were analyzed in triplicate. List of primers is available in **Supplementary Table S1**.

Immunoblot

Total proteins were extracted by directly lysing the cells in Co-IP lysis buffer (100mmol/L NaCl, 50mmol/L Tris pH 7.5, 1mmol/L EDTA, 0.1% Triton X-100) supplemented with 1x protease inhibitors and 1x phosphatase inhibitors. Cell lysates were then treated with 1x reducing agent, 1x loading buffer, boiled and loaded onto neutral pH, pre-cast, discontinuous SDS-PAGE mini-gel system. After electrophoresis, proteins were transferred to nitrocellulose membranes using the Trans-Blot Turbo Transfer System (Bio-Rad). The transblotted membranes were blocked for 1 h in TBST 5% milk and then probed with appropriate primary antibodies (from 1:200 to 1:1000) overnight at 4°C. List of antibodies and working concentrations are available in **Supplementary Table S1**. Next, the membranes were incubated for 1 h at room temperature with fluorescent secondary goat anti-mouse (IRDye 680) or anti-rabbit (IRDye 800) antibodies (both from LI-COR Biosciences). Blots were scanned using the Odyssey Infrared Imaging System (LI-COR Biosciences) and band intensity was quantified using ImageJ software. The ratio of proteins of interest/loading control in idasanutlin-treated samples were normalized to their DMSO-treated control counterparts. All experiments were performed and analyzed in triplicate.

Drug treatment

$10x10^3$ exponentially growing cells were plated in a 96-well plate. After 24 h, cells were treated with serial dilution of RG7388-idasanutlin **(Supplementary Table S1)** or dimethyl sulfoxide (DMSO). DMSO served as the drug vehicle, and its final concentration was no more than 0.1%. Cell viability was measured after 72 h using CellTiter-Glo Luminescent Cell Viability Assay reagent. Results were normalized to the vehicle (DMSO). Curve fitting was performed using Prism (GraphPad) software and the nonlinear regression equation.

Proliferation assay

Cell proliferation was assayed using the xCELLigence system (RTCA, ACEA Biosciences) as previously described (50). Background impedance of the xCELLigence system was

measured for 12 s using 50 µl of room temperature cell culture media in each well of E-plate 16. Cells were grown and expanded in tissue culture flasks as previously described (50). After reaching 75% confluence, cells were washed with PBS and detached from the flasks using a short treatment with trypsin/EDTA. 5,000 cells were dispensed into each well of an E-plate 16. Cell growth and proliferation were monitored every 15 min up to 120 h via the incorporated sensor electrode arrays of the xCELLigence system, using the RTCA-integrated software according to the manufacturer's parameters. In the case of transient siRNA transfection, cells were detached and plated on xCELLigence 24 h post-transfection. For all the experiments with idasanutlin (RG7388), the drug or DMSO were added to the cells 24 h post-seeding on the xCELLigence system, as indicated on the figures. All experiments were performed in triplicate. Results are shown as mean ± SD.

Apoptosis analysis by flow cytometry

Cells were collected 72 h post-siRNA transfection and 48 h post-treatment with idasanutlin (RG7388) respectively, stained with annexin V (AnnV) and propidium iodide (PI), and analysed by flow cytometry using the BD FACSCanto II cytometer (BD Biosciences, USA). Briefly, cells were harvested after incubation period and washed twice by centrifugation (1,200g, 5mins) in cold phosphate-buffered saline (DPBS; Gibco, CO; #14040133). After washing, cells were resuspended in 0.1ml AnnV binding buffer 1X containing fluorochrome-conjugated AnnV and PI (PI to a final concentration of 1 µg/ml) and incubated in darkness at room temperature for 15mins. As soon as possible cells were analyzed by flow cytometry, measuring the fluorescence emission at 530 nm and >575 nm. Data were analyzed by FlowJo software version 10.5.3.

Zebrafish xenografts

Animal experiments and zebrafish husbandry were approved by the "Kantonales Veterinaeramt Basel□Stadt" (haltenewilligung: 1024H) in Switzerland and the experiments were carried out in compliance of ethics regulation. Zebrafish were bred and maintained as

described previously (51). Staging was done by hours post fertilization (hpf) as described previously (52) and according to FELASA and Swiss federal law guidelines. Zebrafish wild type Tuebingen strains were used in this study. 48 h post-siRNA transfection, *GATA3*-silenced and control BT-474 cells were treated for 24 h with idasanutlin (25 µM). After harvesting, cells were labeled with a lipophilic red fluorescent dye (CellTracker™ CM DiI), according to the manufacturer's instructions. Zebrafish were maintained, collected, grown and staged in E3 medium at 28.5°C according to standard protocols(53). For xenotransplantation experiments, zebrafish embryos were anesthetized in 0.4% tricaine at 48 h (hpf) and 200 *GATA3*-silenced or control BT-474 cells were micro-injected into the vessel-free area of the yolk sac. After injection, embryos were incubated for 1 h at 28.5–29°C for recovery and cell transfer verified by fluorescence microscopy. Embryos were examined for the presence of a fluorescent cell mass localized at the injection site in the yolk sac or hindbrain ventricle. Fish harboring red cells were incubated at 35°C as described previously (31,54). On assay day 4, embryos were screened by fluorescence microscopy for (a) normal morphology, (b) a visible cell mass in the yolk or hindbrain ventricle, using a Zeiss SteREO Discovery V20 microscope and the number of tumor-bearing fish quantified. The screening was performed independently by two scientists. For each condition, 70 to 100 fish were analyzed over two experiments. Representative pictures were taken using a Nikon CSU-W1 spinning disk microscope. To assess cell proliferation, fish were furthermore dissociated into single cells as described previously (55,56) and the number of fluorescence-labeled cells was then determined using flow cytometry on a BD FACSCanto II cytometer for CM-DiI–positive cells. For each condition, 20 to 30 fish were analyzed. Each experiment was repeated twice.

Chorioallantoic membrane (CAM)

Fertilized chicken eggs were obtained from Gepro Geflügelzucht AG at day 1 of gestation and were maintained at 37°C in a humidified (60%) incubator for nine days (57) At this time, an artificial air sac was formed using the following procedure: a small hole was drilled

through the eggshell into the air sac and a second hole near the allantoic vein that penetrates the eggshell membrane. A mild vacuum was applied to the hole over the air sac in order to drop the CAM. Subsequently, a square 1cm window encompassing the hole near the allantoic vein was cut to expose the underlying CAM (57). After the artificial air sac was formed, BT-474 cells growing in tissue culture were inoculated on CAMs at 2×10^6 cells per CAM, on three to four CAMs each. Specifically, 48 h post-siRNA transfection, *GATA3*-silenced and control BT-474 cells were treated with idasanutlin (25 µM). 24 h post-treatment, cells were detached from the culture dish with Trypsin, counted, suspended in 20 µl of medium (DMEM) and mixed with an equal volume of Matrigel. To prevent leaking and spreading of cells, a 8mm (inner diameter) sterile teflon ring (removed from 1.8 ml freezing vials, Nunc, Denmark) was placed on the CAMs and the final mixture was grafted onto the chorioallantoic membranes inoculating the cells with a pipette inside the ring (58). Embryos were maintained at 37□°C for 4 days after which tumors at the site of inoculation were excised using surgical forceps. Images of each tumor were acquired with a Canon EOS 1100D digital camera. Surface measurements were performed by averaging the volume (height*width*width) of each tumor using ImageJ, as previously described (59). Total n≥10 tumors for each condition were analyzed over three independent experiments.

Immunohistochemistry

Tumors were fixed in 10% Paraformaldehyde (PFA) immediately after excision from the CAM. PFA-fixed and paraffin-embedded tumors were cut as 3.5 µm thick sections. Hematoxylin and eosin (H&E) staining was performed according to standard protocols. Tissue sections were rehydrated and immunohistochemical staining was performed on a BOND-MAX immunohistochemistry robot (Leica Biosystems) with BOND polymer refine detection solution for DAB, using anti-GATA3, cleaved caspase 3, phospho-Akt or phospho-S6 **(Supplementary Table S1)** primary antibodies as substrate. Photomicrographs of the tumors were acquired using an Olympus BX46 microscope. All stained sections were

evaluated blindly by two independent pathologists.

RNA sequencing and pathway analysis

Biological duplicates were generated for all the samples analyzed. Total RNA was extracted from cells at 75% confluence using TRIZOL **(Supplementary Table S1)** according to the manufacturer's guidelines. RNA samples were treated with Turbo DNase (AM 1907, Thermo Fisher Scientific) and quantified using a Qubit Fluorometer (Life Technologies). RNA integrity was measured using the Agilent Bioanalyzer 2100 (Agilent Technologies).

Library generation was performed using the TruSeq Stranded mRNA protocol (Illumina). Paired-end RNA sequencing was performed on the Illumina NovaSeq 6000 platform using the 2x100bp protocol according to the manufacturer's guidelines. Reads were aligned to the GRCh37 human reference genome using STAR 2.7.1 (60), and transcript quantification was performed using RSEM 1.3.2 (61). Genes without at least ten assigned reads in at least two samples were discarded. Counts were normalized using the median of ratios method from the DESeq2 package (62) in R version 3.6.1 (https://www.R-project.org/). Differential expression analysis was performed using the DESeq2 Wald test. Gene set enrichment analysis was performed using the *fgsea* R package (63) and the Hallmark gene set from the Molecular Signatures Database (64), using the ranked t statistics from the DESeq2 Wald test. Pathways with false discovery rate (FDR) < 0.05 were considered to be significant. Results were visualized using ggplot2 (65).

Analysis of The Cancer Genome Atlas (TCGA) data

ER-positive breast cancer mutation annotation file for variant calling pipeline mutect2, FPKM gene expression data and raw read counts of the TCGA BRCA project were downloaded using *TCGAbiolinks (66)* package. Tumor samples were classified as *GATA3*-mutant (n=122) and *GATA3*-wild type (n=596) according to the *GATA3* mutation status. Samples

with *GATA3* mRNA expression in the bottom and top quartile were classified as *GATA3*-low (n=200) and *GATA3*-high (n=204), respectively. *edgeR* package (67) was used for differential expression analysis and the genes with low expression (<1 log-counts per million in ≥ 30 samples) were filtered out. Normalization was performed using the "TMM" (weighted trimmed mean) method

(68) and differential expression was assessed using the quasi-likelihood F-test. Gene set enrichment analysis of all analyzed genes ranked based on signed p-value according to the direction of the log-fold change was performed using the *fgsea* package (63). Hallmark gene sets from Molecular Signatures Database (64) were used to identify significantly up-/down-regulated pathways. Pathways with FDR < 0.05 were considered significantly regulated.

Analysis of mutual exclusive genetic alterations

ER-positive breast cancer mutational data for the *GATA3, TP53, PIK3CA* and *PTEN* genes and copy number status for *PTEN* derived from the TCGA PanCancer Atlas(1) and the METABRIC dataset (19) were obtained using cBioportal (69). A total of 2379 samples were used for the analysis. Mutual exclusivity of somatic mutations in *GATA3, TP53, PIK3CA* and *PTEN* and deep deletions for *PTEN* were calculated using one-sided Fisher's Exact and *P*<0.05 was considered statistically significant.

Quantification and statistical analysis

Statistical analyses were conducted using Prism software v7.0 (GraphPad Software, La Jolla, CA, USA). For *in vitro* studies, statistical significance was determined by the two-tailed unpaired Student's t-test. For comparison involving multiple time points, statistical significance was determined by the two-tailed unpaired multiple Student's t-test. A *P* value < 0.05 was considered statistically significant. For all figures, ns, not significant. For *in vivo* studies two-sided Fisher's Exact was used to compare the number of tumor-harboring fish. For the CAM assay a two-tailed unpaired Student's t-test was used. The statistical parameters (i.e., exact value of n, p values) have been noted in the figures. Unless otherwise

indicated, all data represent the mean ± standard deviation from at least three independent experiments.

Power calculation

For the *in vivo* experiments the samples size was calculated using a G*Power calculation (70). For zebrafish experiments, assuming a difference of 20% in tumorigenic potential and type I error of 5%, 85 samples in each group would ensure >80% power to detect statistical differences between experimental groups using Fisher's exact test. Furthermore, assuming a 95% engraftment rate, 95 experiments would ensure we had >95% probability of having 85 successful xenotransplantations.

For the CAM assay, assuming an effect size of 1.5 and type I error of 5%, 9 samples in each group would ensure >80% power to detect statistical differences between experimental groups using unpaired t-tests. Furthermore, assuming a 95% engraftment rate, 10 experiments would ensure we had >91% probability of having 9 successful xenotransplantations

Data availability

RNA-sequencing data are available at the NCBI Sequence Read Archive (PRJNA623723).

Code availability

Scripts used to generate the figures for the analysis of the RNA-sequencing are available on request from the corresponding authors.

Acknowledgments

We would like to thank Stefano Medagli who helped with the generation of the figures and Dr. Federica Panebianco for the scientific discussion. We would like to thank Dr. Rachael

Natrajan for sharing breast cancer cell lines. RNA-sequencing analysis was performed at sciCORE scientific computing center at the University of Basel.

Author contributions: C.K.Y.N. and S.P. conceived and supervised the study, interpreted the results, wrote and edited the manuscript with G.B. and M.C.-L.; G.B., M.C.-L., C.K.Y.N. and S.P. made final edits, figures and completed the paper; G.B., M.C.-L., S.T.-M., and V.P. performed molecular experiments and collected the data; M.K., M.D.M, M.K.-D.J., and C.L. provided the technical expertise for the *in vivo* experiments performed by G.B., M.C.-L, S.T.-M and M.K.; S.S., H.M. and N.B. developed the statistical model for the analysis of the DRIVE data; C.E. and L.M.T. analyzed the histological stains and provided pathology expertise; J.G. and V.K. performed bioinformatic analysis of the RNA-sequencing and the publicly available data; R.M.J. provided the *ESR1* mutant models and provided critical input in the discussion of the results. All authors agreed to the final version of the manuscript.

References

1. Hoadley KA, Yau C, Hinoue T, Wolf DM, Lazar AJ, Drill E, et al. Cell-of-Origin Patterns Dominate the Molecular Classification of 10,000 Tumors from 33 Types of Cancer. Cell. 2018;173:291–304.e6.

2. Bertucci F, Ng CKY, Patsouris A, Droin N, Piscuoglio S, Carbuccia N, et al. Genomic characterization of metastatic breast cancers. Nature. 2019;569:560–4.

3. Kouros-Mehr H, Slorach EM, Sternlicht MD, Werb Z. GATA-3 maintains the differentiation of the luminal cell fate in the mammary gland. Cell. 2006;127:1041–55.

4. Chou J, Lin JH, Brenot A, Kim J-W, Provot S, Werb Z. GATA3 suppresses metastasis and modulates the tumour microenvironment by regulating microRNA-29b expression. Nat Cell Biol. 2013;15:201–13.

5. Zaret KS, Carroll JS. Pioneer transcription factors: establishing competence for gene expression. Genes Dev. 2011;25:2227–41.

6. Theodorou V, Stark R, Menon S, Carroll JS. GATA3 acts upstream of FOXA1 in mediating ESR1 binding by shaping enhancer accessibility. Genome Res. 2013;23:12–22.

7. Liu J, Prager–van der WJ, Look MP, Sieuwerts AM, Smid M, Meijer–van Gelder ME, et al. GATA3 mRNA expression, but not mutation, associates with longer progression-free survival in ER-positive breast cancer patients treated with first-line tamoxifen for recurrent disease. Cancer Lett. 2016;376:104–9.

8. Mehra R, Varambally S, Ding L, Shen R, Sabel MS, Ghosh D, et al. Identification of GATA3 as a breast cancer prognostic marker by global gene expression meta-analysis. Cancer Res. 2005;65:11259–64.

9. Gulbahce HE, Sweeney C, Surowiecka M, Knapp D, Varghese L, Blair CK. Significance

of GATA-3 expression in outcomes of patients with breast cancer who received systemic chemotherapy and/or hormonal therapy and clinicopathologic features of GATA-3-positive tumors. Hum Pathol. 2013;44:2427–31.

10. Ashworth A, Lord CJ. Synthetic lethal therapies for cancer: what's next after PARP inhibitors? [Internet]. Nature Reviews Clinical Oncology. 2018. page 564–76. Available from: http://dx.doi.org/10.1038/s41571-018-0055-6

11. Bryant HE, Schultz N, Thomas HD, Parker KM, Flower D, Lopez E, et al. Specific killing of BRCA2-deficient tumours with inhibitors of poly(ADP-ribose) polymerase. Nature. 2005;434:913–7.

12. McDonald ER 3rd, de Weck A, Schlabach MR, Billy E, Mavrakis KJ, Hoffman GR, et al. Project DRIVE: A Compendium of Cancer Dependencies and Synthetic Lethal Relationships Uncovered by Large-Scale, Deep RNAi Screening. Cell. 2017;170:577–92.e10.

13. Chan EM, Shibue T, McFarland JM, Gaeta B, Ghandi M, Dumont N, et al. WRN helicase is a synthetic lethal target in microsatellite unstable cancers. Nature. 2019;568:551–6.

14. Lieb S, Blaha-Ostermann S, Kamper E, Rippka J, Schwarz C, Ehrenhöfer-Wölfer K, et al. Werner syndrome helicase is a selective vulnerability of microsatellite instability-high tumor cells. Elife [Internet]. 2019;8. Available from: http://dx.doi.org/10.7554/eLife.43333

15. Srivatsa S, Montazeri H, Bianco G, Coto-Llerena M, Ng CKY, Piscuoglio S, et al. Discovery of synthetic lethal interactions from large-scale pan-cancer perturbation screens [Internet]. Available from: http://dx.doi.org/10.1101/810374

16. Momand J, Zambetti GP, Olson DC, George D, Levine AJ. The mdm-2 oncogene product forms a complex with the p53 protein and inhibits p53-mediated transactivation. Cell. 1992;69:1237–45.

17. Wade M, Li Y-C, Wahl GM. MDM2, MDMX and p53 in oncogenesis and cancer therapy. Nat Rev Cancer. 2013;13:83–96.

18. Barretina J, Caponigro G, Stransky N, Venkatesan K, Margolin AA, Kim S, et al. The Cancer Cell Line Encyclopedia enables predictive modelling of anticancer drug sensitivity. Nature. 2012;483:603–7.

19. Pereira B, Chin S-F, Rueda OM, Vollan H-KM, Provenzano E, Bardwell HA, et al. The somatic mutation profiles of 2,433 breast cancers refines their genomic and transcriptomic landscapes. Nat Commun. 2016;7:11479.

20. Dydensborg AB, Rose AAN, Wilson BJ, Grote D, Paquet M, Giguère V, et al. GATA3 inhibits breast cancer growth and pulmonary breast cancer metastasis. Oncogene. 2009;28:2634–42.

21. Yan W, Cao QJ, Arenas RB, Bentley B, Shao R. GATA3 inhibits breast cancer metastasis through the reversal of epithelial-mesenchymal transition. J Biol Chem. 2010;285:14042–51.

22. Ding Q, Zhang Z, Liu J-J, Jiang N, Zhang J, Ross TM, et al. Discovery of RG7388, a potent and selective p53-MDM2 inhibitor in clinical development. J Med Chem. 2013;56:5979–83.

23. Reis B, Jukofsky L, Chen G, Martinelli G, Zhong H, So WV, et al. Acute myeloid leukemia patients' clinical response to idasanutlin (RG7388) is associated with pre-treatment MDM2 protein expression in leukemic blasts. Haematologica. 2016;101:e185–8.

24. Pan R, Ruvolo V, Mu H, Leverson JD, Nichols G, Reed JC, et al. Synthetic Lethality of Combined Bcl-2 Inhibition and p53 Activation in AML: Mechanisms and Superior Antileukemic Efficacy [Internet]. Cancer Cell. 2017. page 748–60.e6. Available from: http://dx.doi.org/10.1016/j.ccell.2017.11.003

25. Robinson DR, Wu Y-M, Vats P, Su F, Lonigro RJ, Cao X, et al. Activating ESR1 mutations in hormone-resistant metastatic breast cancer. Nat Genet. 2013;45:1446–51.

26. Hartmaier RJ, Trabucco SE, Priedigkeit N, Chung JH, Parachoniak CA, Vanden Borre P, et al. Recurrent hyperactive ESR1 fusion proteins in endocrine therapy-resistant breast cancer. Ann Oncol. 2018;29:872–80.

27. Jeselsohn R, Bergholz JS, Pun M, Cornwell M, Liu W, Nardone A, et al. Allele-Specific Chromatin Recruitment and Therapeutic Vulnerabilities of ESR1 Activating Mutations. Cancer Cell. 2018;33:173–86.e5.

28. Kuang Y, Siddiqui B, Hu J, Pun M, Cornwell M, Buchwalter G, et al. Unraveling the clinicopathological features driving the emergence of ESR1 mutations in metastatic breast cancer [Internet]. npj Breast Cancer. 2018. Available from: http://dx.doi.org/10.1038/s41523-018-0075-5

29. White R, Rose K, Zon L. Zebrafish cancer: the state of the art and the path forward. Nat Rev Cancer. 2013;13:624–36.

30. Fior R, Póvoa V, Mendes RV, Carvalho T, Gomes A, Figueiredo N, et al. Single-cell functional and chemosensitive profiling of combinatorial colorectal therapy in zebrafish xenografts. Proc Natl Acad Sci U S A. 2017;114:E8234–43.

31. Haldi M, Ton C, Seng WL, McGrath P. Human melanoma cells transplanted into zebrafish proliferate, migrate, produce melanin, form masses and stimulate angiogenesis in zebrafish. Angiogenesis. 2006;9:139–51.

32. Hagedorn M, Javerzat S, Gilges D, Meyre A, de Lafarge B, Eichmann A, et al. Accessing key steps of human tumor progression in vivo by using an avian embryo model. Proc Natl Acad Sci U S A. 2005;102:1643–8.

33. Fluegen G, Avivar-Valderas A, Wang Y, Padgen MR, Williams JK, Nobre AR, et al.

Phenotypic heterogeneity of disseminated tumour cells is preset by primary tumour hypoxic microenvironments. Nat Cell Biol. 2017;19:120–32.

34. Wu X, Bayle JH, Olson D, Levine AJ. The p53-mdm-2 autoregulatory feedback loop. Genes Dev. 1993;7:1126–32.

35. Khoo KH, Verma CS, Lane DP. Drugging the p53 pathway: understanding the route to clinical efficacy [Internet]. Nature Reviews Drug Discovery. 2014. page 217–36. Available from: http://dx.doi.org/10.1038/nrd4236

36. Marcellino B, Cassinat B, Farnoud N, Lu M, Verger E, McGovern E, et al. Expansion of Prior Existing TP53 Mutated Clones in Polycythemia Vera Patients Treated with Idasanutlin [Internet]. Blood. 2019. page 838–838. Available from: http://dx.doi.org/10.1182/blood-2019-128342

37. Miyamoto H, Izumi K, Yao JL, Li Y, Yang Q, McMahon LA, et al. GATA binding protein 3 is down-regulated in bladder cancer yet strong expression is an independent predictor of poor prognosis in invasive tumor. Hum Pathol. 2012;43:2033–40.

38. Nguyen AHT, Tremblay M, Haigh K, Koumakpayi IH, Paquet M, Pandolfi PP, et al. Gata3 antagonizes cancer progression in Pten-deficient prostates. Hum Mol Genet. 2013;22:2400–10.

39. Feng Z, Zhang H, Levine AJ, Jin S. The coordinate regulation of the p53 and mTOR pathways in cells. Proc Natl Acad Sci U S A. 2005;102:8204–9.

40. Vousden KH, Lu X. Live or let die: the cell's response to p53 [Internet]. Nature Reviews Cancer. 2002. page 594–604. Available from: http://dx.doi.org/10.1038/nrc864

41. Werner S, Brors B, Eick J, Marques E, Pogenberg V, Parret A, et al. Suppression of early hematogenous dissemination of human breast cancer cells to bone marrow by retinoic Acid-induced 2. Cancer Discov. 2015;5:506–19.

42. Yu W, Huang W, Yang Y, Qiu R, Zeng Y, Hou Y, et al. GATA3 recruits UTX for gene transcriptional activation to suppress metastasis of breast cancer. Cell Death Dis. 2019;10:832.

43. Miller TW, Hennessy BT, González-Angulo AM, Fox EM, Mills GB, Chen H, et al. Hyperactivation of phosphatidylinositol-3 kinase promotes escape from hormone dependence in estrogen receptor–positive human breast cancer [Internet]. Journal of Clinical Investigation. 2010. page 2406–13. Available from: http://dx.doi.org/10.1172/jci41680

44. Kojima K, Shimanuki M, Shikami M, Samudio IJ, Ruvolo V, Corn P, et al. The dual PI3 kinase/mTOR inhibitor PI-103 prevents p53 induction by Mdm2 inhibition but enhances p53-mediated mitochondrial apoptosis in p53 wild-type AML. Leukemia. 2008;22:1728–36.

45. Moreno-Smith M, Lakoma A, Chen Z, Tao L, Scorsone KA, Schild L, et al. p53 Nongenotoxic Activation and mTORC1 Inhibition Lead to Effective Combination for Neuroblastoma Therapy. Clin Cancer Res. 2017;23:6629–39.

46. Nagata Y, Lan K-H, Zhou X, Tan M, Esteva FJ, Sahin AA, et al. PTEN activation contributes to tumor inhibition by trastuzumab, and loss of PTEN predicts trastuzumab resistance in patients. Cancer Cell. 2004;6:117–27.

47. Jordan JJ, Inga A, Conway K, Edmiston S, Carey LA, Wu L, et al. Altered-function p53 missense mutations identified in breast cancers can have subtle effects on transactivation. Mol Cancer Res. 2010;8:701–16.

48. Uphoff CC, Drexler HG. Detecting mycoplasma contamination in cell cultures by polymerase chain reaction. Methods Mol Biol. 2011;731:93–103.

49. Livak KJ, Schmittgen TD. Analysis of Relative Gene Expression Data Using Real-Time Quantitative PCR and the 2−ΔΔCT Method. Methods. 2001;25:402–8.

50. Andreozzi M, Quintavalle C, Benz D, Quagliata L, Matter M, Calabrese D, et al. HMGA1 Expression in Human Hepatocellular Carcinoma Correlates with Poor Prognosis and Promotes Tumor Growth and Migration in in vitro Models. Neoplasia. 2016;18:724–31.

51. Nusslein-Volhard C, Dahm R. Zebrafish. Oxford University Press; 2002.

52. Kimmel CB, Warga RM, Schilling TF. Origin and organization of the zebrafish fate map. Development. 1990;108:581–94.

53. Choi J, Dong L, Ahn J, Dao D, Hammerschmidt M, Chen J-N. FoxH1 negatively modulates flk1 gene expression and vascular formation in zebrafish [Internet]. Developmental Biology. 2007. page 735–44. Available from: http://dx.doi.org/10.1016/j.ydbio.2007.01.023

54. Konantz M, Balci TB, Hartwig UF, Dellaire G, André MC, Berman JN, et al. Zebrafish xenografts as a tool for in vivo studies on human cancer [Internet]. Annals of the New York Academy of Sciences. 2012. page 124–37. Available from: http://dx.doi.org/10.1111/j.1749-6632.2012.06575.x

55. Svoboda O, Stachura DL, Machonova O, Zon LI, Traver D, Bartunek P. Ex vivo tools for the clonal analysis of zebrafish hematopoiesis. Nat Protoc. 2016;11:1007–20.

56. Carapito R, Konantz M, Paillard C, Miao Z, Pichot A, Leduc MS, et al. Mutations in signal recognition particle SRP54 cause syndromic neutropenia with Shwachman-Diamond-like features. J Clin Invest. 2017;127:4090–103.

57. Zijlstra A, Mellor R, Panzarella G, Aimes RT, Hooper JD, Marchenko ND, et al. A quantitative analysis of rate-limiting steps in the metastatic cascade using human-specific real-time polymerase chain reaction. Cancer Res. 2002;62:7083–92.

58. Kim J, Yu W, Kovalski K, Ossowski L. Requirement for specific proteases in cancer cell intravasation as revealed by a novel semiquantitative PCR-based assay. Cell.

1998;94:353–62.

59. Lauzier A, Normandeau-Guimond J, Vaillancourt-Lavigueur V, Boivin V, Charbonneau M, Rivard N, et al. Colorectal cancer cells respond differentially to autophagy inhibition in vivo. Sci Rep. 2019;9:11316.

60. Dobin A, Davis CA, Schlesinger F, Drenkow J, Zaleski C, Jha S, et al. STAR: ultrafast universal RNA-seq aligner. Bioinformatics. 2013;29:15–21.

61. Li B, Dewey CN. RSEM: accurate transcript quantification from RNA-Seq data with or without a reference genome [Internet]. BMC Bioinformatics. 2011. Available from: http://dx.doi.org/10.1186/1471-2105-12-323

62. Love MI, Huber W, Anders S. Moderated estimation of fold change and dispersion for RNA-seq data with DESeq2. Genome Biol. 2014;15:550.

63. Sergushichev AA. An algorithm for fast preranked gene set enrichment analysis using cumulative statistic calculation [Internet]. Available from: http://dx.doi.org/10.1101/060012

64. Liberzon A, Birger C, Thorvaldsdóttir H, Ghandi M, Mesirov JP, Tamayo P. The Molecular Signatures Database Hallmark Gene Set Collection [Internet]. Cell Systems. 2015. page 417–25. Available from: http://dx.doi.org/10.1016/j.cels.2015.12.004

65. Wickham H. ggplot2 [Internet]. 2009. Available from: http://dx.doi.org/10.1007/978-0-387-98141-3

66. Colaprico A, Silva TC, Olsen C, Garofano L, Cava C, Garolini D, et al. TCGAbiolinks: an R/Bioconductor package for integrative analysis of TCGA data. Nucleic Acids Res. 2016;44:e71.

67. Robinson MD, McCarthy DJ, Smyth GK. edgeR: a Bioconductor package for differential expression analysis of digital gene expression data [Internet]. Bioinformatics. 2010.

page 139–40. Available from: http://dx.doi.org/10.1093/bioinformatics/btp616

68. Robinson MD, Oshlack A. A scaling normalization method for differential expression analysis of RNA-seq data. Genome Biol. 2010;11:R25.

69. Cerami E, Gao J, Dogrusoz U, Gross BE, Sumer SO, Aksoy BA, et al. The cBio cancer genomics portal: an open platform for exploring multidimensional cancer genomics data. Cancer Discov. 2012;2:401–4.

70. Faul F, Erdfelder E, Lang A-G, Buchner A. G*Power 3: A flexible statistical power analysis program for the social, behavioral, and biomedical sciences [Internet]. Behavior Research Methods. 2007. page 175–91. Available from: http://dx.doi.org/10.3758/bf03193146